A Self-Adjusting Sinusoidal Power Source Suitable for Driving Capacitive Loads

Sam Ben-Yaakov* and Mor Mordechai Peretz
Power Electronics Laboratory
Department of Electrical and Computer Engineering
Ben-Gurion University of the Negev
P.0.Box 653, Beer-Sheva 84105, ISRAEL
Tel: +972-8-6461561; Fax: +972-8-6472949
Email: sby@ee.bgu.ac.il ; Website: http://www.ee.bgu.ac.il/~pel

***Abstract*—A new self-adjusting current-fed push-pull parallel inverter (SA-CFPPRI) is presented and tested by simulation and experimentally. The power source includes a soft switching control circuitry and a controllable inductor. The SA-CFPPRI can drive a capacitive load at any frequency within the design range. It will maintain zero voltage switching of the main transistors and follow the input frequency signal even when the resonant elements and/or the load vary. Possible range of applications for the proposed power source is: piezoelectric transformers and motors, ac bus for a distributed power system and other loads that need to be fed by a sinusoidal waveform. The experimental results of the laboratory unit (160Vrms at 93kHz and nominal output power of 5W) verify the analytical analysis and proposed design procedure.**

Keywords: Push-Pull Parallel Resonant Inverter; Variable inductor; Phase comparator; Sinusoidal Power Source.

I. INTRODUCTION

The favorable drive signal for a number of capacitive loads is a sinusoidal waveform. For example, piezoelectric devices and in particular piezoelectric motors need to be driven by a high frequency sinusoidal waveform [1-6]. This is required since the optimal performance is obtained when the drive is of low harmonics contents.

Capacitive loads pose a number of non-trivial power electronics design problems. The major one being the reactive current that may reduce dramatically the efficiency if it is allowed to pass through the power switches. Another problem is the need to accommodate load changes (both the active and reactive parts) without affecting the amplitude, waveform and efficiency of the power driver. The Current-Fed Push-Pull Resonant Inverter (CFPPRI) [7] was shown earlier to be a useful topology for driving capacitive load [5]. However, the basic CFPPRI suffers from a number of drawbacks that will reduce the efficiency and increase distortion if the load capacitance or operating frequency is non-constant. In this study we explored the possibility of converting the CFPPRI into a self-adjusting system that will accommodate load capacitance changes and frequency shifts without increasing the losses or distorting the waveform fed to the load.

II. THE CURRENT-FED PUSH-PULL PARALLEL RESONANT INVERTER (CFPPRI)

The basic CFPPRI topology (Fig. 1) includes a push-pull stage with two transistors (Q_1, Q_2) driving a parallel resonant network and fed by a series inductor L_{in}. The load (capacitive in this case) is fed via a secondary winding that allows for amplitude adjustment by the turns ratio ($n_2/2n_1$). The resonant frequency (f_r) of the parallel resonant network will be :

$$f_r = \frac{1}{2\pi\sqrt{L_m \sum C_2}} \qquad (1)$$

where L_m is the secondary inductance and $\sum C_2$ is the total capacitance reflected to the secondary ($C_1(n_2/2n_1)^2 + C_2 + C_L$).

When the gate drive frequency of the CFPPRI, fs, matches the resonant frequency, fr, the transistors will operate under Zero Voltage Switching (ZVS) conditions (Fig. 2a) and in this case the reactive current of the equivalent resonant network will not pass through the switches. This is the most desirable case. If the frequency of the gate drives is lower than the resonant frequency (Fig. 2b), the operation will include a "Boost" period in which one transistor and one antiparallel diode are carrying the inductor current [8, 9]. This will cause distortion in the output voltage and will increase the conduction losses. If the gate drive frequency is higher than the resonant frequency (Fig. 2c), the operation will be under hard switching conditions. This will cause distortion of the load signal and will introduce switching losses. In many practical applications, an exact matching of the resonant elements to the gate drive frequency (and the desired output frequency) is not possible. Interconnecting cable capacitances, tolerances of the passive components and the variability of the load capacitance will cause the CFPPRI stage to operate in one of the mismatched modes, which would be highly undesirable in some applications such as piezoelectric motors.

The sensitivity of the CFPPRI to deviation of the drive frequency from the resonant frequency can be remedied by locking the drive frequency to the resonant frequency. That is, to make the gate drive frequency equal to the resonant

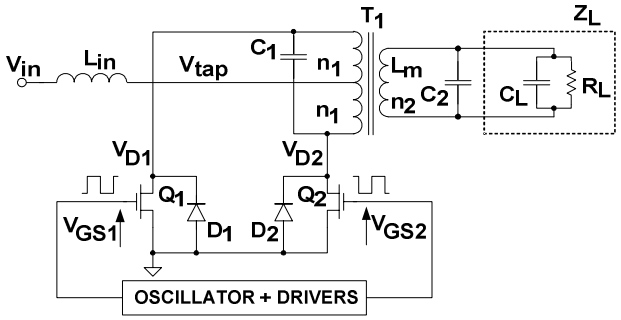

Figure 1. Basic configuration of the CFPPRI loaded by a capacitive load.

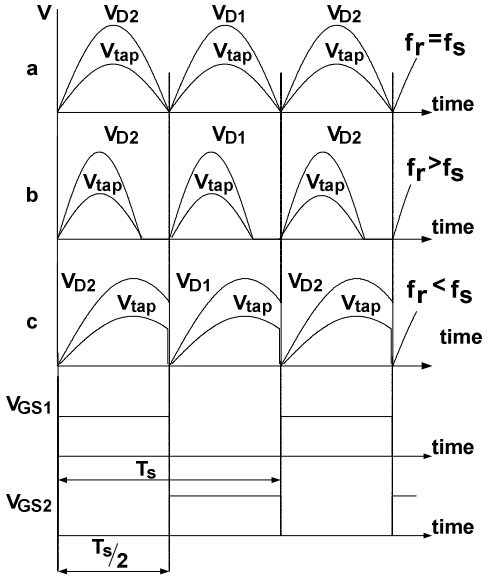

Figure 2. Gate voltages (VGS), drain voltages (VD) and tap voltage (Vtap) when the gate-drive frequency matches the resonant frequency (a) and when it is lower (b) or higher (c) than the resonant frequency.

frequency. This converts, in fact, the operation from a driven to a self-driven CFPPRI configuration [7] except that an active driver is included and an active comparator is used to detect the zero crossing (Fig. 3). This Soft Switching Control (SSC) method is employed in commercial controllers/drivers (e.g. UC3872 by Texas Instruments) that include all the associated circuitry - such as a starting and protection circuitries.

The SSC ensures ZVS even if the inductance and total capacitance of the resonant network are non-constant since it forces the gate drive frequency to match the resonant frequency. However if the load needs to be driven at a pre-determined frequency, the SSC solution, by itself, is not sufficient. This deficiency is solved in proposed approach by applying a variable inductor [10, 11].

III. The Self-Adjusting CFPPRI (SA-CFPPRI)

By including both a SSC and a variable inductor, the CFPPRI can be made to operate at a desired switching frequency and at the same time maintain ZVS. The variable high frequency inductor presented earlier [10] is based on an E core with a gapped center leg and bias windings on the non-gapped side legs (Fig. 4). The self-adjusting operation is achieved by including into the CFPPRI the variable inductor and introducing a buck type converter, for feeding the bias windings. Frequency tracking is accomplished by closing the loop on a phase comparator that generates an error signal as function of a phase mismatch between the desired frequency and the SA-CFPPRI frequency (Fig. 5).

The bias drive of the SA-CFPPRI is designed as a closed feedback loop configuration to maintain a forced current control. This is required to reduce the order of the outer feedback loop. The simplified block diagram of the SA-CFPPRI (Fig. 6) includes therefore two feedback loops: an inner current loop and an outer phase loop.

Starting from left side, K_p represents the gain of the phase comparator while the blocks 'Int' stand for the integration operation that transfers frequency into phase. H_1 is the phase comparator's output filter designed to be of the lag-lead type (Fig. 5). G_1 and G_2 are the gains of the summing amplifier A_1. K_M (Fig. 6) is the transfer ratio of the modulator (error signal to duty cycle). B is the transfer function of the Buck converter, (duty cycle to current). T is the transfer ratio of the pulse transformer and H_2 is the pulse transformer filter. H_L is the relationship between the bias current and the inductance of the bias winding n_3 of T_1 (Fig. 5). And finally, K_f is the response of the tank to the bias current (the ratio of resonant frequency to bias current).

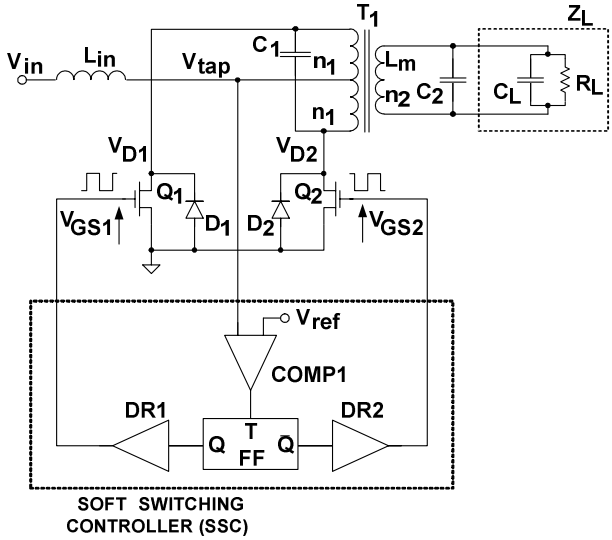

Figure 3. Soft switching controller (SSC) for a CFPPRI.

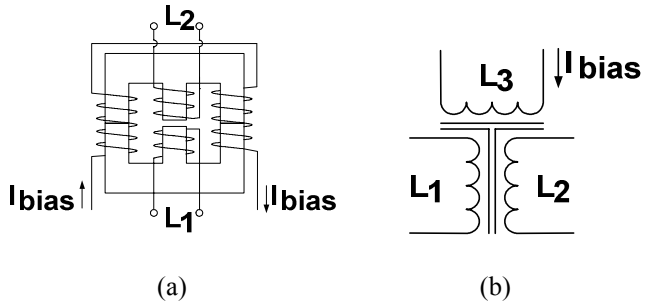

Figure 4. The variable inductor (a) and its schematics symbol (b).

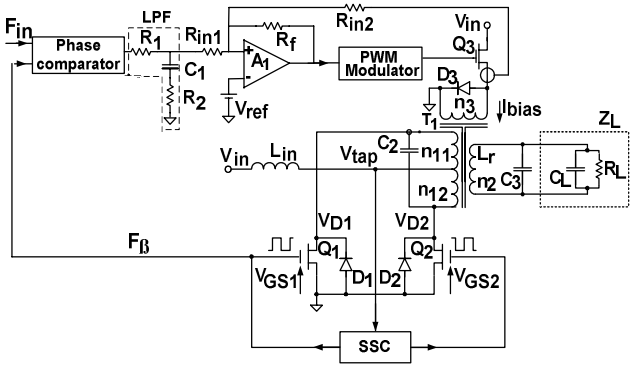

Figure 5. Basic configuration of the SA-CFPPRI.

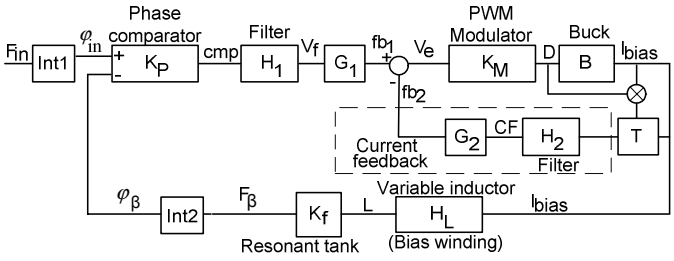

Figure 6. Simplified control block diagram of proposed SA-CFPPRI.

When considering the low frequency response of the system, K_P, G_1, G_2, K_M, H_L and K_f (Fig. 6) can be assumed to be fast responding as compared to H_1 (response of phase comparator filter) and B (Buck converter). Without current feedback around the Buck converter, the system will be of a second order form and therefore hard to stabilize. This is because the transfer function from error signal to inductor current is expected to be a first order system and when in series with integrator (Int2, Fig. 6) the loop gain of the system will be of the second order form. Current feedback is implemented (Fig. 7a) by sensing the switch current of the buck converter with a current transformer, filtering the signal by a R-C network and feeding the signal back to the summing amplifier A1 (Figs. 5, 6). The bias inductor current can be expressed as:

$$I_{bias} = \frac{DV_{in}}{sL_{b0}} \tag{2}$$

where L_{b0} is the bias inductor value for a given operating condition and D is the duty cycle of the buck converter. After linearization, the small signal transfer function between duty cycle and the inductor current b, is expressed as:

$$b(s) = \frac{i_{bias}}{d} = \frac{V_{in}}{sL_{b0}} \tag{3}$$

where, i_{bias} is the small signal inductor current and d is the duty cycle perturbation.

Since the current is sensed at the switch branch (Fig. 5), the average current feedback signal I_f can be expressed as :

$$I_f(av) = \frac{DI_{bias}}{n} \tag{4}$$

where n is the turns ratio of the current transformer. Applying again linearization around the operating point (denoted by the subscript 0) we find the expression for the small signal average feedback current (i_f(av)):

$$i_f(av) = \frac{dI_{bias0}}{n} + \frac{i_{bias}D_0}{n}. \tag{5}$$

Hence, the small signal equivalent circuit of the current sensing circuitry (T and B in Fig. 6) can be represented by Fig. 7b. The voltage feedback signal v_{CF} that will develop at the output of the current sense filter will thus be:

$$v_{CF}(s) = \left[d\frac{I_0}{n} + i_{bias}\frac{D_0}{n} \right] \frac{R_{14}}{sC_{11}R_{14}+1}. \tag{6}$$

Combining (3) and (6) yields:

$$v_{CF}(s) = \left[d\frac{I_0}{n} + d\frac{V_{in}}{sL_{b0}}\frac{D_0}{n} \right] \frac{R_{14}}{sC_{11}R_{14}+1}. \tag{7}$$

Consequently, the transfer function v_{CF} to d, (cf(s)) can now be expressed as:

$$cf(s) = \frac{v_{CF}}{d}(s) = \left[\frac{V_{in}}{sL_{b0}} \right] \left[\frac{D_0 R_{14}}{n} \left[s\left(\frac{L_{b0}I_0}{V_{in}D_0} \right) + 1 \right] \frac{R_{14}}{sC_{11}R_{14}+1} \right]. \tag{8}$$

It should be noted that this equation combined the effect of B (the Buck converter), (T the pulse transformer) and H_2 (the pulse transformer filter) (Fig. 6).

For a given nominal operating point, one can design the feedback as a frequency independent gain by pole zero cancellation:

$$s\left(\frac{L_{b0}I_0}{V_{in}D_0} \right) + 1 = \frac{R_{14}}{sC_{11}R_{14}+1}. \tag{9}$$

Isolating C_{11}, yields the flat filter transfer function criterion:

$$C_{11} = \frac{L_{b0}I_0}{V_{in}D_0R_{14}}. \tag{10}$$

Note that the resistor R_{14} also controls the total gain of the block. Once R_{14} is chosen, C_{11} value can be selected according to (10).

Taking into account G_2 (error amplifier gain) and K_M (modulator's transfer ratio) (Fig. 6), the closed loop transfer function of the Buck converter from the output of H_1, v_f (Fig. 6) to the bias current i_{bias}, $A_{CL\_CL}(s)$ is:

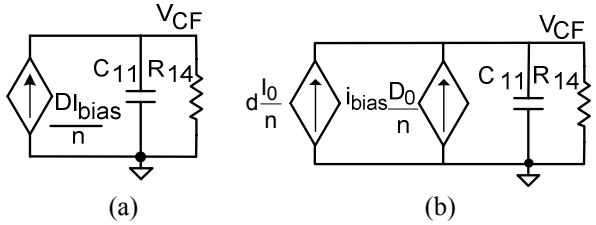

Figure 7. The current feedback circuitry including the current transformer.(a) Large signal. (b) Small signal.

$$A_{CF\_CL}(s) = \frac{i_{bias}}{v_f} = \frac{G_1 K_M b}{1 + G_2 K_M cf} \quad (11)$$

where K_M, b, , G_2 are the current loop transfer functions and G_1 is the error amplifier gain (Fig. 6).

Inserting (8) into (11) one gets:

$$A_{CF\_CL}(s) = \frac{G_1 K_M b}{1 + \frac{D_0 R_{14} K_M}{n} G_2 b \left[s \frac{L_{b0} I_0}{V_{in} D_0} + 1 \right] \frac{1}{sC_{11}R_{14} + 1}}. \quad (12)$$

And for the case of the pole-zero cancellation (10):

$$A_{CF\_CL}(s) = \frac{G_1 K_M b}{1 + bG_2 K_M \frac{D_0 R_{14}}{n}}. \quad (13)$$

Applying (3) and selecting G_1 to be equals to G_2, eq. (13) reduces to a first order system with a bandwidth of ω_{CL}:

$$A_{CF\_CL}(s) = \frac{A_{CL0}}{1 + s/\omega_{CL}} \quad (14)$$

where

$$A_{CL0} = \frac{n}{DR_{14}}$$

$$\omega_{CL} = G_2 K_M \frac{D_0 R_{14}}{n} \frac{V_{in}}{L_{b0}}$$

Equation (14) implies that for the frequency range $\omega < \omega_{CL}$, the current feedback has transformed the buck converter (from error signal to bias current) from a first order system to a zero order system. If the parameters of (13) are chosen such that the bandwidth ω_{CL} of the current converter is larger than the bandwidth of the overall system then the closed loop response of the system f_β/f_{in} $A_{PF\_CL}(s)$ can be expressed as:

$$A_{PF\_CL}(s) = \frac{f_\beta}{f_{in}}(s) = \frac{1}{s} \frac{A_{PF}}{1 + \beta_{PF} A_{PF}} \quad (15)$$

where

$$A_{PF} = K_p H_1 G_1 A_{CF\_CL} K_f H_L$$

$$\beta_{PF} = \frac{1}{s}$$

After some manipulation the closed loop transfer function of the system can be shown as a first order system of bandwidth ω_0:

$$A_{PF\_CL}(s) = \frac{A_{SYS0}}{1 + s/\omega_0} \quad (16)$$

where

$$A_{SYS0} = 1$$

$$\omega_0 = K_p h_1 G_1 A_{CF\_CL} K_f H_L$$

The parameter h_1 in above expression stands for the transfer function of the phase detector filter H_1 (Fig. 6) at frequencies close to ω_0. H_1 is designed to be a lag-lead network (Fig. 5) and the zero is placed to be below ω_0. Consequently, h_1 will be flat at frequencies around ω_0.

IV. Simulation and Experimental Results

A prototype SA-CFPPRI was designed, simulated, built and tested experimentally (a detailed circuit diagram is given in Fig. 8). The target parameters of the experimental units were: Input voltage: 11VDC; Output voltage: Vout = 160 Vrms; Nominal output power: 5W; Load capacitance range: C_L = 1.1nF – 9.1 nF; Frequency range: f_{in} = 80 kHz – 150 kHz.

Transformer characteristics were: Core type: ETD29; Magnetizing inductance (secondary side): L_m = 1.5mH; Turns ratio: n_2:n_{11} = n_2:n_{12} = 3:20; n_3= 80 turns. The behavior of the variable inductor is given in Fig. 7. The inner current loop was designed to have a bandwidth of 6 kHz. The over all closed loop response of the system was designed to have a bandwidth of about 3 kHz with a nominal output capacitance of 2.1nF at a carrier frequency of 93kHz.

Typical waveforms of the experimental unit are given in Fig. 9. The operational range of the prototype is summarized in Fig. 10. The experimentally measured bias currents and calculated inductances are given in Fig. 11. The closed loop step response of the system is given in Fig. 12 and was found to be in good agreement with the simulated one shown in Fig. 13.

The efficiency of the experimental unit (taking into account the total input power to power stage and control section) was found to be about 67% when the inductors bias current was low and about 52% when the variable inductor was forced to its minimum value (highest bias current).

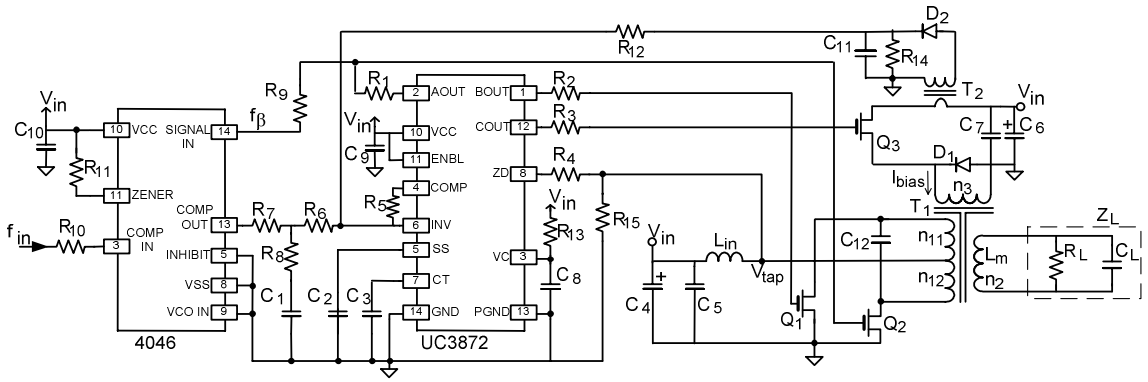

Figure 8. Complete experimental circuit setup.

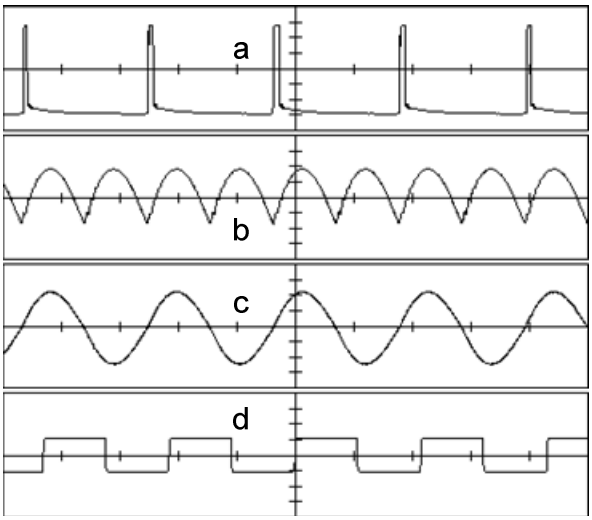

Figure 9. Experimental results. (a) Control pulses to bias Buck converter (2V/div). (b) VD1 (5V/div). (c) output voltage (100 V/div). (d) Input frequency signal (5 V/div). Horizontal scale (5µs/div.)

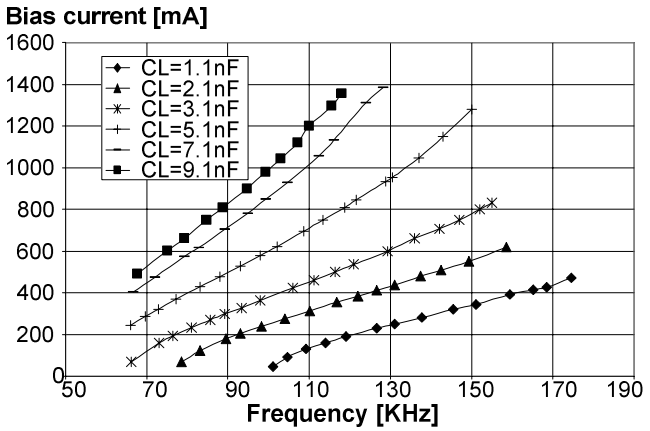

Figure 10. Measured bias current as a function of operating frequency for various load capacitances of experimental unit.

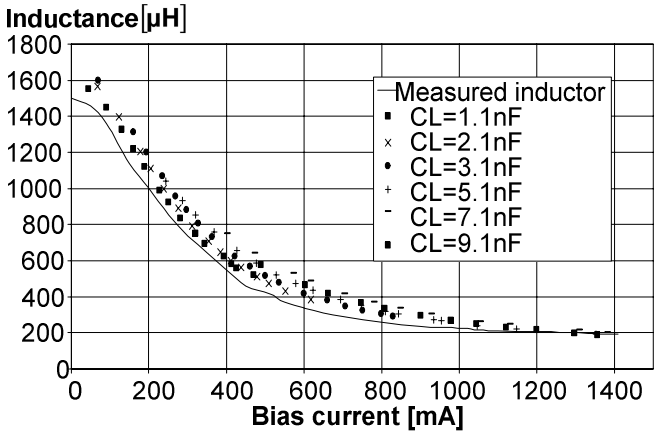

Figure 11. Inductance of variable inductor as a function of bias current. Measured (solid line) and calculated from experimental results.

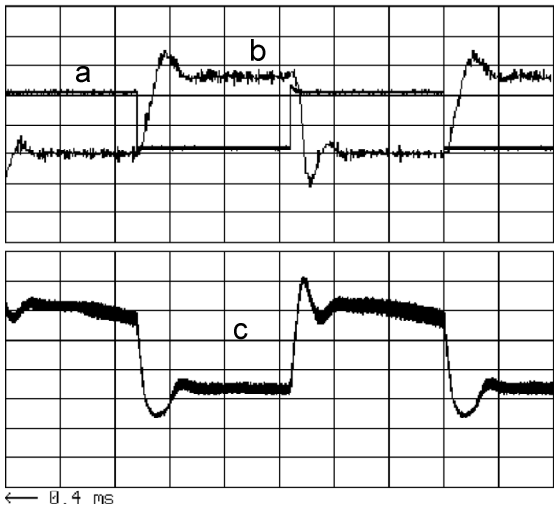

Figure 12. Measured response of experimental unit to a step in input frequency around 93 KHz (with output capacitance of 2.1 nF). (a) Modulating signal (b) Output frequency change (1.56 kHz/div). (c) Error signal at the output of phase detector filter (H1) of Fig. 5 (20.5 mV/div). Horizontal scale: 1 (ms/div). (b) was measured the frequency jitter (Jfreq)feature of the Lecroy WaveRunner digital oscilloscope.

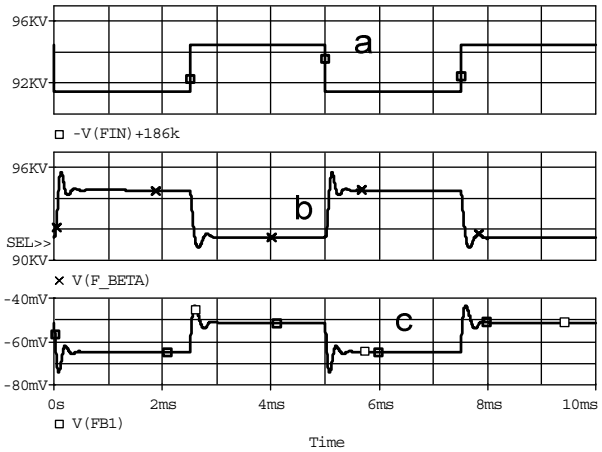

Figure 13. Simulated response of experimental unit to a step in input frequency around 93 KHz (with output capacitance of 2.1 nF). (a) Modulating signal (b) Output frequency change. (c) Error signal at the output of phase detector filter (H1) of Fig. 5.

V. Discussion and Conclusions

The proposed SA-CFPPRI was shown to be able to drive variable capacitive loads under ZVS for any drive frequency (within the operation range of the design). For a variable inductor that can be controlled over some m:1 ratio, the range of allowed load capacitor variation that the SA-PRRI will accommodate is also about m:1. It is expected that the system should be able to drive inductive loads as long as the variable inductor can be controlled to keep the tank in resonance for the given drive frequency. Amplitude control can be easily incorporated by another Buck stage that will feed the input

series inductor. The operating frequency range of the system can be adjusted by selecting the nominal value for the variable inductor.

The relative reactive power of the system, circulating in the tank (but not passed by the transistors) is a function of the quality factor Q of the system that is, $\omega_s L/R_L$. For proper operation, Q should be relatively high (Q>5). This implies that this approach is perhaps limited to low or medium power (hundreds of Watts) and may not be practical to high power applications due to the very high current that need to handled by the tank. This is especially true for high operating frequency because the size of high frequency high current inductor will be large given the available core materials. This situation, however, is not different from that of any other resonant inverter.

A possible application of proposed SA-CFPPRI includes drivers for piezoelectric motors. The advantages of using SA-CFPPRI in this case are: the generation of a sinusoidal wave with low distortion, the ability to compensate for device capacitance changes and interconnecting cables capacitances, and the relatively high efficiency. The latter is due to the fact that the resonant current is locked at the secondary and does not pass through the switches, and the fact that ZVS is automatically maintained. The over all efficiency measured for the experiment system is modest but is maintained constant over the whole frequency range. Without a self adjusting, controllable inductor, reasonable efficiency can be obtained at one frequency only – the frequency that matches the resonant frequency of the fixed inductor. At high frequencies, when the bias current needs to be high so as to lower the inductance, the efficiency is expected (and was measured) to drop due to increased losses of the bias section. The losses include two parts: copper losses of the bias winding and Buck converter losses. The relatively low efficiency that was observed at large bias currents is evidently due to converter losses. These can possibly be improved by a better design of the bias Buck converter. In particular, synchronous rectification and soft switching could be beneficial.

Another benefit of the SA-CFPPRI as a piezoelectric motor driver is the compatibility with optimizing control schemes. For example, by adding a frequency sweep arrangement one can lock to the optimal frequency in terms of efficiency, torque or speed.

The proposed approach that is based on the variable inductor and the SSC circuitry could be useful in other applications, such as for driving an ac distributed system bus or driving resistive loads (e.g. fluorescent lamp) when the drive frequency need to be constant or controlled.

ACKNOWLEDGMENT

This research was supported by THE ISRAEL SCIENCE FOUNDATION grant # 113/02-1.

REFERENCES

[1] G W. R. Chynoweth, J. F. Elliott, H. W. Katz, E. B. Mullen, C. A. Rosen, N. Schwarz, B. Silverman, C. F. Spitzer, S. W. Tehon, and H. J. Venema, "Solid state magnetic and dielectric devices", *John Wiley & Sons, Inc.,* New York, 1959.

[2] H. P. Shoner, "Piezoelectric motors and their application", *European Trans. on Electric Power Engineering,* vol. 2, no. 6, 367-371, 1992.I. S. Jacobs and C. P. Bean, "Fine particles, thin films and exchange anisotropy," in Magnetism, vol. III, G. T. Rado and H. Suhl, Eds. New York: Academic, 1963, pp. 271–350.

[3] J. A. Martín-Ramos, M. A. J. Prieto, F. Nuño García, J. Díaz Gonzáles, and F. M. F. Linera, "A new full-protected control mode to drive piezoelectric transformers in DC-DC converters", *IEEE Trans. on Power Electronics,* vol. 17, no. 6, 1096-1103, 2002.

[4] Y. Ishizuka, Kao-Wan Lee, T. Oyama, H. Matsuo, and T. Koga, "Consideration of a single-switch inverter for piezoelectric transformer with a new control method", *IEEE Power Electronics Specialists Conference, PESC-03,* 1621-1626, Acapulco-México, 2003.

[5] S. Ben-Yaakov, E. Rozanov, T. Wasserman, T. Rafaeli, L. Shiv, and G. Ivensky, "A resonant driver for a piezoelectric motor with single transistor direction switches", *IEEE Applied Power Electronics Conference, APEC-2000*, 1037-1043, New Orleans, 2000.

[6] M. Gulko and S. Ben-Yaakov, "Current-sourcing parallel-resonance inverter (CS-PPRI): Theory and application as a discharge lamp driver", *IEEE Trans. on Industrial Electronics*, vol. 41, no. 3, 285-291, 1994.

[7] M. Jordan and J. A. O'Connor, "Resonant Fluorescent Lamp Converter Provides Efficient and Compact Solution," *Conference Record of IEEE-APEC,* 424-431, 1993.

[8] G. Ivensky, A. Abramovitz, M. Gulko, and S. Ben-Yaakov, "A resonant DC-DC transformer", *IEEE Trans. on Aerospace and Electronic Systems*, vol. 29, no. 3, 926-934, San Diego, 1993.

[9] J. A. Sierra and W. Kaiser**,** "Comparison of fluorescent lamp stabilization methods in the current-fed push-pull inverter," *Industry Applications Conference- IAS*, Vol. 3, 2099 -2104, 1998.

[10] D. Medini and S. Ben-Yaakov, "A current controlled variable inductor for high frequency resonant power circuits", *IEEE Applied Power Electronics Conference, APEC-94*, 219-225, Orlando, 1994.

[11] M. Gulko, D. Medini, and S. Ben-Yaakov, "Inductor-controlled current-sourcing resonant inverter and its application as a high pressure discharge lamp driver", IEEE Applied Power Electronics Conference, APEC-94, 434-440, Orlando, 1994.